

# Hadronic $\gamma Z$ box corrections in Møller scattering

N. L. Hall<sup>a</sup>, P. G. Blunden<sup>b</sup>, W. Melnitchouk<sup>c</sup>, A. W. Thomas<sup>a</sup>, R. D. Young<sup>a</sup>

<sup>a</sup>*ARC Centre of Excellence for Particle Physics at the Terascale and CSSM, School of Chemistry and Physics,  
University of Adelaide, Adelaide SA 5005, Australia*

<sup>b</sup>*Department of Physics and Astronomy, University of Manitoba, Winnipeg, MB, Canada R3T 2N2*

<sup>c</sup>*Jefferson Lab, 12000 Jefferson Avenue, Newport News, Virginia 23606, USA*

---

## Abstract

The possibility of measuring the parity-violating asymmetry in Møller scattering with sufficient accuracy to determine  $\sin^2 \theta_W$  to 0.1% offers a complementary path to the discovery of new physics to that followed at high energy colliders. We present a new calculation of the  $\gamma Z$  box contribution to parity-violating electron-proton scattering, which constitutes an important uncertainty in computing the background to this process. We show that while the  $\gamma Z$  correction grows rapidly with energy, it can be relatively well constrained by data from parity-violating inelastic scattering and parton distribution functions.

*Key words:* Parity violation, weak charge of the proton, Møller scattering, parity-violating inelastic scattering

---

## 1. Introduction

In the search for physics beyond the Standard Model, low-energy precision tests of parity violation (PV) provide crucial alternatives to searches at colliders such as those at the Large Hadron Collider. Following pioneering work at SLAC [1] and MIT-Bates [2], Jefferson Lab has recently seen several such experiments. The first, involving elastic electron–proton scattering [3–5], led to the determination of the strangeness contribution to the nucleon electromagnetic form factors [6, 7], as well as significant new limits on the quark weak couplings  $C_{1u}$  and  $C_{1d}$  [8, 9]. More recently, the first report from the  $Q_{\text{weak}}$  experiment [10] significantly improved those limits, while a final, higher precision result is expected soon. The most recent experiment involved the measurement of inelastic electron–deuteron scattering in the nucleon resonance region and beyond [11]. All of these experiments were completed using Jefferson Lab’s 6 GeV polarised electron beam and served to test the running of  $\sin^2 \theta_W$  at low  $Q^2$ . Following the 12 GeV upgrade of the CEBAF accelerator, a new generation of PV experiments, such as MOLLER [12] and SoLID [13], will provide even more stringent constraints on the Standard Model.

In this Letter we examine the Møller scattering process, and in particular the  $\gamma Z$  radiative corrections to the background  $ep$  scattering, which presents one of the main theoretical uncertainties to this process. The MOLLER experiment will scatter longitudinally polarised electrons from atomic electrons in a liquid hydrogen target with the aim of measuring the weak charge of the electron,  $Q_W^e$ , to within 2.3% [12]. This will be equivalent to determining  $\sin^2 \theta_W$  to  $\approx 0.1\%$ , placing it on par with the two (different) values for  $\sin^2 \theta_W$  measured at the  $Z$  pole. This is especially important since these two values differ by  $3\sigma$ , and, although their average is consistent with other experimental data, if either of them were found to be the correct value, the behaviour of  $\sin^2 \theta_W$  would change markedly [12] from that expected within the Standard Model. Even if the average were indeed correct at the  $Z$  boson pole, a measurement to this precision would provide important information on the nature of possible new physics [12, 14, 15].

The PV asymmetry in Møller scattering is defined as

$$A_{\text{PV}} = \frac{\sigma_+ - \sigma_-}{\sigma_+ + \sigma_-}, \quad (1)$$

where  $\sigma_\lambda$  is the cross section for an incoming right-handed (helicity  $\lambda = +1$ ) or left-handed (helicity  $\lambda = -1$ ) electron. At the kinematics relevant to the MOLLER experiment, the asymmetry is dominated by the

interference between the tree-level  $\gamma$  and  $Z$  exchanges, and is given by [16],

$$A_{\text{PV}} = m_e E \frac{G_F}{\sqrt{2}\pi\alpha} \frac{2y(1-y)}{1+y^4+(1-y)^4} Q_W^e, \quad (2)$$

where  $m_e$  and  $E$  are the incident electron's mass and energy, respectively,  $y$  is the fractional energy transferred,  $G_F$  is the Fermi constant and  $\alpha$  the fine structure constant. At tree (or Born) level the weak charge of the electron is given by  $Q_W^{e(\text{Born})} = -1 + 4\sin^2\theta_W$ . For a determination of  $Q_W^e$  to a precision of  $\approx 2.3\%$ , higher order radiative corrections must also be included. These have been calculated in Refs. [17–19] using standard techniques.

Because the MOLLER experiment uses a hydrogen target, the measurement of the PV asymmetry unavoidably includes a background contribution from PV  $ep$  scattering, which depends on the weak charge of the proton,  $Q_W^p$ . The  $Q_{\text{weak}}$  experiment should determine the effective (or energy-dependent) proton weak charge to an accuracy of 4% at an energy of 1.165 GeV, where the overall radiative corrections shift the Born result by around 75%. Of particular importance is the  $\gamma Z$  box contribution associated with the vector coupling of the  $Z$  boson at the proton (axial-vector coupling at the electron),  $\Box_{\gamma Z}^V$ . While this constitutes a modest,  $\approx 7\%$  correction to  $Q_W^p$  at the  $Q_{\text{weak}}$  energy, it initially grows linearly with energy and is found to be significantly more important ( $\approx 15\%$ ) at the MOLLER energy of  $E = 11$  GeV.

In fact, there has been considerable interest recently in accurately computing the absolute value and uncertainty of the  $\Box_{\gamma Z}^V$  correction [20–25], particularly how it impacts the interpretation of the  $Q_{\text{weak}}$  experiment. The most recent analysis [25] used the Adelaide-Jefferson Lab-Manitoba (AJM) model [25] to provide a precise determination of the  $\gamma Z$  correction, utilising constraints from PV  $ed$  inelastic scattering data [11] and global parton distribution functions (PDFs). Since it is essential for the MOLLER experiment that the total error on the proton weak charge at 11 GeV be less than 4%, it is necessary to ensure that the  $\Box_{\gamma Z}^V$  correction here also is under control. Unfortunately, to date there has been no estimate of this correction at the kinematics relevant to the MOLLER experiment. We do so in this Letter.

## 2. Adelaide-Jefferson Lab-Manitoba model

In presenting our calculation of the  $\gamma Z$  correction to the inelastic background for the MOLLER experiment, we begin by briefly summarising the salient features of the AJM model as relevant for the present analysis; further details can be found in Ref. [25]. At tree level, the weak charge of the proton is given by  $Q_W^{p(\text{Born})} = 1 - 4\sin^2\theta_W$ , while at higher orders additional radiative corrections are important, the most challenging of which is the  $\gamma Z$  interference box term,  $\Box_{\gamma Z}^V$ . From the crossing symmetry properties of the vector hadron part of the  $\gamma Z$  correction, the real part of  $\Box_{\gamma Z}^V$  can be written with the help of a forward dispersion relation in terms of its imaginary part [20],

$$\Re \Box_{\gamma Z}^V(E) = \frac{2E}{\pi} \mathcal{P} \int_0^\infty dE' \frac{1}{E'^2 - E^2} \Im m \Box_{\gamma Z}^V(E'), \quad (3)$$

where  $\mathcal{P}$  denotes the principal value integral. Using the optical theorem, the imaginary part of  $\Box_{\gamma Z}^V$  can be computed from the vector interference  $\gamma Z$  structure functions  $F_{1,2}^{\gamma Z}$  as [20, 21, 26]

$$\Im m \Box_{\gamma Z}^V(E) = \frac{1}{(s - M^2)^2} \int_{W_\pi^2}^s dW^2 \int_0^{Q_{\text{max}}^2} dQ^2 \frac{\alpha(Q^2)}{1 + Q^2/M_Z^2} \left[ F_1^{\gamma Z} + \frac{x s (Q_{\text{max}}^2 - Q^2)}{Q^4} F_2^{\gamma Z} \right], \quad (4)$$

where  $Q^2$  is (minus) the squared mass of the exchanged virtual  $\gamma$  or  $Z$  boson,  $W$  is the invariant mass of the hadronic intermediate state, and  $x = Q^2/(W^2 - M^2 + Q^2)$  is the Bjorken scaling variable, with  $M$  the nucleon mass, and  $M_Z$  the mass of the  $Z$  boson. The  $W^2$  integration ranges from the pion threshold,  $W_\pi^2 = (M + m_\pi)^2$ , up to the total center of mass energy squared,  $s = M^2 + 2ME$ , while the upper limit on the  $Q^2$  integration is  $Q_{\text{max}}^2 = 2ME(1 - W^2/s)$ . Because there is little or no experimental data on the interference  $F_{1,2}^{\gamma Z}$  structure functions at the kinematics most relevant to this integral, these need to be estimated from phenomenological models.

Following Ref. [22], we divide the integral in Eq. (4) into separate regions in  $Q^2$  and  $W^2$  according to the dominant physical features and mechanisms that characterise each region. In particular, at low  $Q^2$  and  $W^2$

( $Q^2 \leq 10 \text{ GeV}^2$  for  $W_\pi^2 \leq W^2 \leq 4 \text{ GeV}^2$  and  $Q^2 \leq 2.5 \text{ GeV}^2$  for  $4 < W^2 \leq 9 \text{ GeV}^2$ , ‘Region I’), the structure functions are dominated by nucleon resonances; at low  $Q^2$  but high  $W^2$  ( $Q^2 \leq 2.5 \text{ GeV}^2$  and  $W^2 > 9 \text{ GeV}^2$ , ‘Region II’) a description in terms of Regge theory is applicable; and at high  $Q^2$  and  $W^2$  ( $Q^2 > 2.5 \text{ GeV}^2$  and  $W^2 > 4 \text{ GeV}^2$ , ‘Region III’) the deep-inelastic structure functions are well described in terms of universal PDFs.

Construction of the  $F_{1,2}^{\gamma Z}$  structure functions requires firstly choosing appropriate electromagnetic structure functions, and then transforming these into their  $\gamma Z$  analogs. In the AJM model, Region I is well described by the empirical fit to electron–proton cross section data from Ref. [27], which is quoted with 3–5% accuracy. The description of Region II follows Gorchtein *et al.* [23] in using the vector meson dominance (VMD) model together with Regge parametrisations of the high- $W$  behaviour [28, 29]. Finally, in Region III any suitable set of leading twist parton distributions [30] can be utilised, and in practice we employ the fit from Alekhin *et al.* [31].

Since the structure functions can be equivalently represented in terms of the cross sections  $\sigma_i$  for the scattering of transverse ( $i = T$ ) and longitudinal ( $i = L$ ) virtual photons or  $Z$  bosons, it is convenient to separate these into their resonance and nonresonant background contributions,  $\sigma_i = \sigma_i^{(\text{res})} + \sigma_i^{(\text{bgd})}$ . These can then be rotated from  $\gamma\gamma \rightarrow \gamma Z$  independently. For the resonant part, the electromagnetic cross section for the production of a given resonance  $R$  can be modified by the ratio [23]

$$\frac{\sigma_i^{\gamma Z(R)}}{\sigma_i^{\gamma\gamma(R)}} = (1 - 4 \sin^2 \theta_W) - y_R, \quad (5)$$

where the parameter  $y_R$  is computed from the helicity-1/2 and 3/2 nucleon  $\rightarrow R$  transition amplitudes for the proton and neutron [22, 23, 25]. While  $y_R$  can in principle depend on  $Q^2$  in addition to  $W^2$ , it was found in Ref. [23] that the uncertainty introduced by approximating  $y_R$  to be independent of  $Q^2$  is minimal, and well within the errors on the helicity amplitudes from the Particle Data Group [32]. The background contribution to the  $\gamma Z$  cross section, on the other hand, is determined via  $\sigma_i^{\gamma Z(\text{bgd})} = (\sigma_i^{\gamma Z} / \sigma_i^{\gamma\gamma}) \sigma_i^{\gamma\gamma(\text{bgd})}$ , where the ratio of the  $\gamma Z$  to  $\gamma\gamma$  cross sections is computed in the framework of the generalised VMD model [23],

$$\frac{\sigma_i^{\gamma Z}}{\sigma_i^{\gamma\gamma}} = \frac{\kappa_\rho + \kappa_\omega R_\omega^i(Q^2) + \kappa_\phi R_\phi^i(Q^2) + \kappa_C^i R_C^i(Q^2)}{1 + R_\omega^i(Q^2) + R_\phi^i(Q^2) + R_C^i(Q^2)}. \quad (6)$$

Here the parameters  $\kappa_V$  ( $V = \rho, \omega, \phi$ ) are ratios of weak and electric charges, while  $\kappa_C^i$  denotes the ratios of the  $\gamma Z$  to  $\gamma\gamma$  continuum contributions. Similarly,  $R_V^i$  are the transverse and longitudinal ratios of the cross sections for the  $V$  and  $\rho$  meson, with  $R_C^i$  the continuum equivalents. Although the VMD model does not provide the parameters  $\kappa_C^i$ , in the AJM model these were constrained by matching the cross section ratio in Eq. (6) with the ratios of PDFs at the boundaries of Regions I, II and III. This was found [25] to significantly reduce the uncertainties in  $F_{1,2}^{\gamma Z}$  compared with earlier estimates [23].

As a test of its veracity, the predictions of the AJM model for PV inelastic asymmetries were compared [25] with recent *ed* scattering data from the E08-011 experiment [11] at Jefferson Lab in the resonance region at  $Q^2 = (0.76 - 1.47) \text{ GeV}^2$ , as well as with earlier *ep* results from the G0 experiment [33] in the  $\Delta$  resonance region at  $Q^2 = 0.34 \text{ GeV}^2$ . The excellent agreement with the data, which were entirely within the kinematics defined by Region I, provides confidence in the extension of the AJM model to MOLLER energies.

Table 1: Contributions to  $\Re \square_{\gamma Z}^V$  in the AJM model from Regions I, II and III at the kinematics of the  $Q_{\text{weak}}$  ( $E = 1.165 \text{ GeV}$ ) and MOLLER ( $E = 11 \text{ GeV}$ ) experiments.

Region	$\Re \square_{\gamma Z}^V (\times 10^{-3})$	
	$Q_{\text{weak}}$	MOLLER
I	$4.64 \pm 0.35$	$3.04 \pm 0.26$
II	$0.59 \pm 0.05$	$5.26 \pm 0.49$
III	$0.35 \pm 0.02$	$3.18 \pm 0.16$
total	$5.57 \pm 0.36$	$11.5 \pm 0.6$

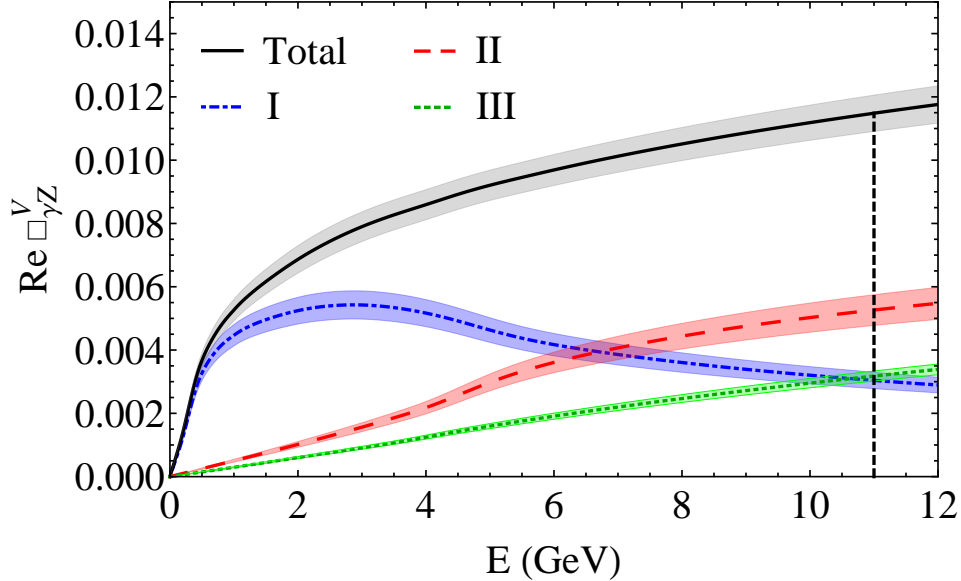


Figure 1: (colour online). Energy dependence of the contributions to  $\Re \square_{\gamma Z}^V$  from the  $W^2$  and  $Q^2$  Regions I (blue dot-dashed line), II (red dashed line), and III (green dotted line), together with the total (black solid line). The vertical line indicates the energy at the MOLLER experiment.

The energy dependence of the calculated  $\Re \square_{\gamma Z}^V$  correction in the AJM model is illustrated in Fig. 1, together with the contributions from the individual regions, and the values of the corrections at the  $Q_{\text{weak}}$  ( $E = 1.165$  GeV) and MOLLER ( $E = 11$  GeV) energies are listed in Table 1. Compared with the correction relevant for  $Q_{\text{weak}}$ , the value of  $\Re \square_{\gamma Z}^V$  is about twice as large at the MOLLER energy, where it is close to one third of the tree level value of  $\sin^2 \theta_W$ . Furthermore, the relative contributions from the various regions also change significantly, especially for Region II, which contributes only  $\approx 11\%$  of the total at the  $Q_{\text{weak}}$  energy, but yields close to 50% of the absolute value at  $E = 11$  GeV. Since Regions I and III contribute less than a third of the total correction, their roles are relatively less important.

### 3. Model dependence

The AJM model as described above provides our best estimate of the energy dependence of  $\Re \square_{\gamma Z}^V$  that is currently possible from existing experimental constraints. It is of course important to ensure that the model dependence of the corrections is accurately reflected in all relevant uncertainties. In this section we investigate the possible model dependence of the most important, Regge contribution from Region II, including the dependence on the structure function parametrisation, and the  $W$  and  $Q^2$  dependence of the continuum VMD parameters  $\kappa_C^i$ .

To identify the most relevant kinematic regions for the calculation, we examine the contributions from various  $Q^2$  and  $W^2$  intervals, illustrated in Fig. 2. At energies  $E \approx 1$  GeV, the low- $Q^2$  region ( $Q^2 < 1$  GeV<sup>2</sup>) dominates the correction, while at  $E \approx 10$  GeV this region makes up only half of the total  $\Re \square_{\gamma Z}^V$ . For the  $W^2$  intervals, the bulk of the integral at lower  $E$  arises from the low- $W$ , nucleon resonance region ( $W \lesssim 2 - 3$  GeV), with larger  $W$  becoming more important with increasing energy. At  $E \approx 10$  GeV, the region  $W^2 > 10$  GeV<sup>2</sup> accounts for nearly two thirds of the total.

For the model dependence of the contribution from Region II, we consider several different models for the  $\gamma Z$  structure functions, each of which is based on parametrisations of electromagnetic cross sections that give reasonable descriptions of the data at low  $W^2$  and high  $Q^2$ , but assuming somewhat different physical mechanisms for the scattering in this region. For example, the Regge theory inspired parametrisation of Capella *et al.* [34] was used in the calculation by Sibirtsev *et al.* [21], while the fit of Alwall and Ingelman [28], based on a combination of the VMD model and Regge phenomenology, was used as the basis of ‘Model II’

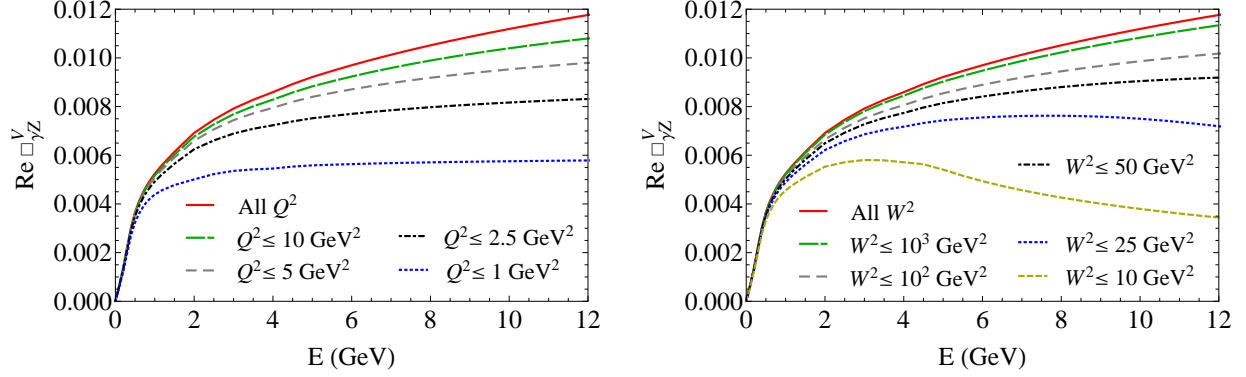


Figure 2: (colour online). Contributions to  $\Re \square_{\gamma Z}^V$  from various kinematic regions in  $Q^2$  (left) and  $W^2$  (right), as a function of the energy  $E$ .

of Gorchtein *et al.* [23]. The colour dipole model (CDP) of Cvetic *et al.* [35, 36] was also used in Ref. [23] in what was referred to as ‘Model I’. Note that while ‘Model I’ considered photon couplings at the hadronic level, ‘Model II’ assumed couplings to quarks directly.

More specifically, in addition to the AJM  $\gamma Z$  structure function model, we compare the results for  $\Re \square_{\gamma Z}^V$  with several alternative models:

#### Modified Regge model (MRM)

As in the original calculation of Ref. [21], the MRM uses the Capella *et al.* parametrisation [34] of  $F_{1,2}^{\gamma\gamma}$ , although instead of using leading twist PDFs to modify the structure functions, here the  $\gamma\gamma \rightarrow \gamma Z$  rotation is performed via Eq. (6). Since this parametrisation is not separated into resonance and nonresonance components, the entire  $F_{1,2}^{\gamma\gamma}$  structure functions must be rotated. This may appear *ad hoc* (since the resonances are all scaled by the same amount), however, because the resonance contribution is negligible in Region II, the total transverse and longitudinal cross sections  $\sigma_i$  are effectively given by their background contributions,  $\sigma_i \approx \sigma_i^{(\text{bgd})}$ .

#### CDP model

The CDP parametrisation of the electromagnetic structure functions [35, 36] formed the basis of ‘Model I’ in Ref. [23]. Instead of using the VMD inspired relation in Eq. (6), however, the  $\kappa_V$  and  $\kappa_C^i$  coefficients were computed from ratios of quark electric charges. The resulting ratio of  $\gamma Z$  to  $\gamma\gamma$  cross sections in this model is then given by a constant value [23],

$$\frac{\sigma_i^{\gamma Z}}{\sigma_i^{\gamma\gamma}} = \frac{9}{5} - 4 \sin^2 \theta_W. \quad (7)$$

In the implementation of the CDP model in the present analysis, an updated parametrisation of the  $\gamma\gamma$  cross section [37] is used.

#### CDP/VMD model

This model combines the electromagnetic structure functions of Cvetic *et al.* [35, 36] with the constrained  $\gamma Z/\gamma\gamma$  ratio in Eq. (6), as in the AJM model. Note that for both the CDP and CDP/VMD models the parametrisation [35, 36] of the structure functions is given only for  $W^2 < 1000 \text{ GeV}^2$ . As shown in Fig. 2, the contribution to the integral from  $W^2 > 1000 \text{ GeV}^2$  is only a very small fraction of the total correction to  $\Re \square_{\gamma Z}^V$ . For the CDP and CDP/VMD models, we estimate the fractional contribution to the integral from the  $W^2 > 1000 \text{ GeV}^2$  region to be the same as in the AJM model.

Using these alternative models for the  $\gamma Z$  interference structure functions, which assume rather different physical pictures, the contributions from Region II to  $\Re \square_{\gamma Z}^V$  are shown in Fig. 3, compared with the results

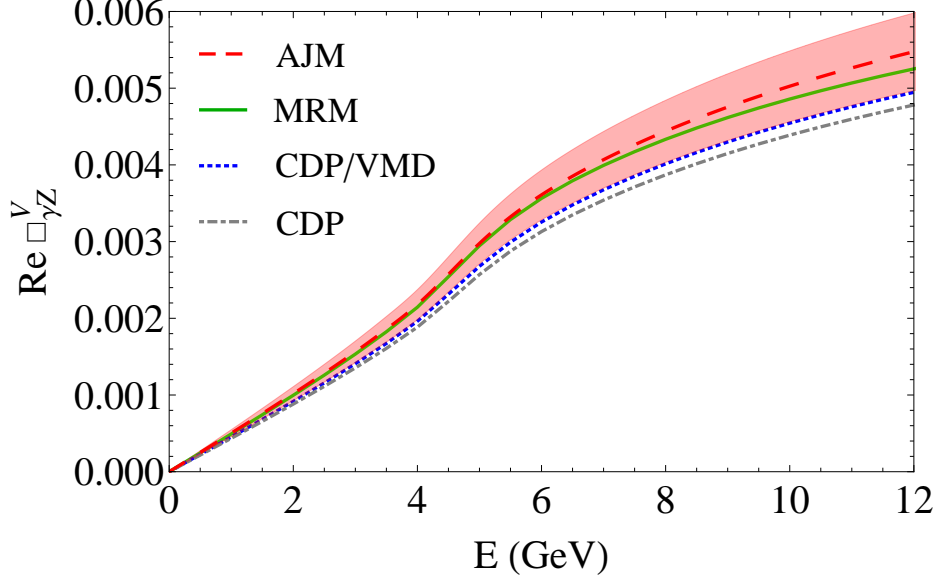


Figure 3: (colour online). Contribution of Region II to  $\Re \square_{\gamma Z}^V$  as a function of energy using various models for the  $\gamma Z$  structure functions: AJM (red dashed line), MRM (green solid line), CDP/VMD (blue dotted line), and CDP (gray dot-dashed line).

of the AJM model of Ref. [25]. The central values of the corrections using the AJM and MRM  $\gamma Z$  structure functions are very similar over the entire range of energies considered, while the CDP and CDP/VMD models give slightly smaller corrections. The uncertainty band of AJM model includes the MRM and CDP/VMD results, with the CDP lying slightly below. To ensure that the overall  $\Re \square_{\gamma Z}^V$  error is not underestimated, we include the full difference between the most disparate central values, combining it in quadrature with the AJM estimate of the error, as an additional uncertainty arising from the model dependence.

A further error on  $\Re \square_{\gamma Z}^V$  could arise from the dependence of the continuum parameters  $\kappa_C^i$  on the invariant hadronic mass  $W$ . In the AJM model, the continuum coefficients were fitted by constant values  $\kappa_C^T = 0.65 \pm 0.14$  and  $\kappa_C^L = -1.3 \pm 1.7$  [25], with the possible  $W^2$  dependence taken into account by appropriate matching over the range between  $W^2 = 4 \text{ GeV}^2$  and  $13 \text{ GeV}^2$ , and including any variation in the uncertainties. Increasing the range over which these are fitted to  $4 \leq W^2 \leq 1000 \text{ GeV}^2$ , one finds  $\kappa_C^T = 0.86 \pm 0.24$  and  $\kappa_C^L = -1.3 \pm 2.3$ , which are consistent with the values obtained in Ref. [25] within the uncertainties. While there is some variation of the resulting  $\gamma Z$  structure functions computed from the two sets of values, the uncertainties assigned to the  $\kappa_C^i$  values in the AJM model are sufficient to cover the different behaviours. Since the additional uncertainty is found to be negligible, we do not assign an additional error on  $\Re \square_{\gamma Z}^V$  from the  $W^2$  dependence of the  $\kappa_C^i$ .

As well as the  $W^2$  dependence, we also consider the  $Q^2$  dependence of the  $\kappa_C^i$  errors in the region  $0 \leq Q^2 \leq 2.5 \text{ GeV}^2$ . Taking the AJM model errors for  $\kappa_C^i$  at  $Q^2 = 2.5 \text{ GeV}^2$ , where the constraints from PDFs are expected to be reliable, the error is increased linearly to 100% at the real photon point,  $Q^2 = 0$ . With these modified constraints the uncertainty on  $\Re \square_{\gamma Z}^V$  would increase from  $\pm 0.36 \times 10^{-3}$  to  $\pm 0.59 \times 10^{-3}$  at the  $Q_{\text{weak}}$  energy, while for MOLLER the error would double to  $\pm 1.2 \times 10^{-3}$ . In either case, these errors would still remain within the experimental budget; in practice, however, we believe they are likely to be too conservative and take the error on  $\kappa_C^T$  to be constant in  $Q^2$ .

Using the AJM model with constraints provided by PDFs, the relative contributions to  $\Re \square_{\gamma Z}^V$  relevant to the MOLLER experiment from the various kinematic regions differ significantly from the those at the  $Q_{\text{weak}}$  energy. In particular, the contribution from Region II is much larger (by  $\sim 50\%$ ) than that at lower energies. Taking into account the additional model dependence discussed in this section, the final value for  $\Re \square_{\gamma Z}^V$  at the MOLLER energy is estimated to be

$$\Re \square_{\gamma Z}^V = (11.5 \pm 0.6 \pm 0.6) \times 10^{-3}, \quad (8)$$

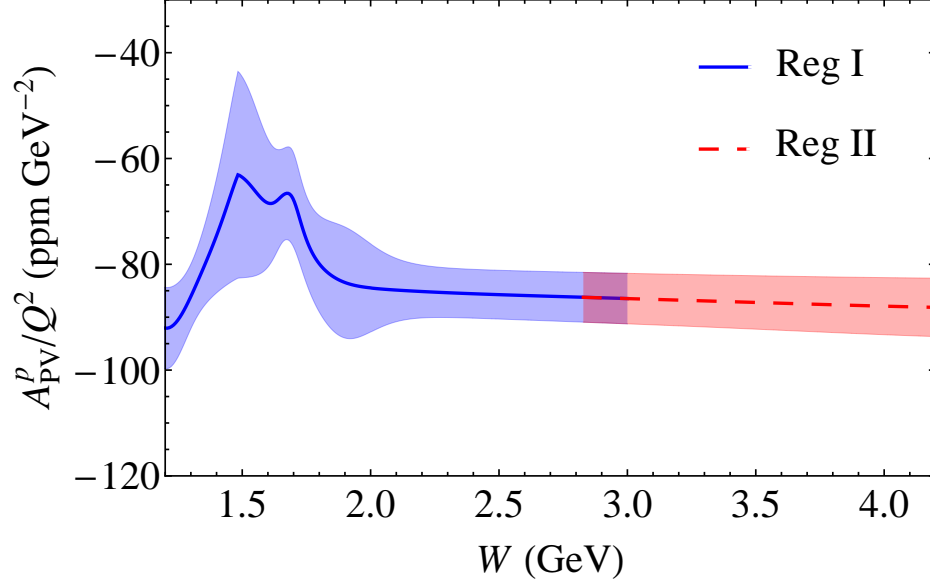


Figure 4: (colour online). PV asymmetry  $A_{PV}^p$  for inelastic  $ep$  scattering, scaled by  $1/Q^2$ , at  $E = 11$  GeV in the AJM model, showing the matching of the contributions from Region I (blue solid line) and Region II (red dashed line). The typical momentum transfer relevant to the MOLLER experiment is  $\approx 0.004$  GeV $^2$ .

where the first error includes the various sources of uncertainty in the AJM model, while the second arises from the additional model dependence considered in this analysis. Further experiments to determine the  $\gamma Z$  interference structure functions would naturally increase the precision of this result. Nevertheless, with the current precision of  $\Re \square_{\gamma Z}^V$ , the effective weak charge of the proton increases from  $0.0757 \pm 0.0007$  at  $E = 1.165$  GeV to  $0.0814 \pm 0.0010$  at  $E = 11$  GeV. Included in this effective  $Q_W^p$  is the contribution from the hadronic axial-vector piece (with leptonic vector coupling to the  $Z$ ),  $\square_{\gamma Z}^A$ . By extending the work of Refs. [24, 38],  $\square_{\gamma Z}^A$  decreases from  $0.0037(2)$  at  $E = 1.165$  GeV to  $0.0035(2)$  at  $E = 11$  GeV. Since PV  $ep$  elastic scattering is estimated to constitute a background of the order 8% to the Møller measurement, the uncertainty it will induce is  $\approx 0.1\%$ . This figure is well below the limit of 0.3% anticipated from elastic proton, as reported in the experimental proposal.

#### 4. Inelastic asymmetry

For the MOLLER experiment, the inelastic  $ep$  cross section is an order of magnitude smaller than the elastic background, yet the inelastic  $Z$  coupling to the proton is not suppressed by the proton weak charge  $Q_W^p$ . This increases the relative significance of this inelastic contribution to the asymmetry, and therefore important to consider.

Within the dispersion relation approach, the main uncertainty in the calculation of  $\Re \square_{\gamma Z}^V$  is the  $\gamma Z$  interference structure functions. In principle these can be measured directly in parity-violating deep-inelastic scattering. In fact, the inelastic PV asymmetry involves the same combination of  $F_{1,2}^{\gamma Z}$  as that appearing in the integrand of Eq. (4), and has been used to constrain the  $\gamma Z$  box corrections. As discussed above, the AJM model makes full use of the available data on PV inelastic  $ep$  [33] and  $ed$  [11] scattering at low and intermediate  $Q^2$  values, in addition to constraints from parton distributions at high  $W$  and  $Q^2$ .

The PV inelastic asymmetry for  $ep$  scattering is shown in Fig. 4 in the AJM model for kinematics typical for the MOLLER experiment, for which  $Q^2 \approx 0.004$  GeV $^2$ . At low  $W$  ( $W \lesssim 2$  GeV) the asymmetry illustrates the structure characteristic of the nucleon resonance region, while at higher  $W$  the asymmetry (scaled by  $1/Q^2$ ) remains approximately constant at  $\approx 85$  ppm/GeV $^2$ , with an uncertainty of  $\approx 7\%$  in the AJM model.

As discussed in the previous section, a more conservative error estimate could amplify the uncertainties on the  $\kappa_C^i$  to 100% at the photon point. In this case, the relative uncertainty on the inelastic PV asymmetry

in the MOLLER experiment would increase to about 25%. It will be important, therefore, to have additional PV inelastic data to further constrain the model, and to empirically constrain the inelastic background in the MOLLER experiment itself. Such direct monitoring of the inelastic  $ep$  asymmetry was achieved in the E158 experiment at SLAC, where this background was resolved at better than 20% precision [39].

Note also that in this estimate other standard radiative corrections to PV inelastic scattering have not been included. These may modify the specific  $W$  distribution shown in Fig. 4; however, for the purposes of illustrating the behaviour of the asymmetry and its uncertainty our estimate is sufficient.

## 5. Conclusion

In summary, we have calculated the energy dependent  $\gamma Z$  radiative correction to PV elastic  $ep$  scattering to an accuracy of  $\approx 7\%$ , at an energy of  $E = 11$  GeV relevant for the planned MOLLER experiment at Jefferson Lab. In contrast to the  $Q_{\text{weak}}$  experiment kinematics, where the resonance region dominates, the energy-dependent  $\text{Re} \square_{\gamma Z}^V$  correction at MOLLER kinematics is much more sensitive to the Regge region. With careful attention paid to the model dependence of the  $\gamma Z$  structure functions in the Regge region, we determine an effective proton weak charge of  $0.0814 \pm 0.0010$  at 11 GeV. This represents a precision that is sufficient to keep the uncertainty from this background within the limits of the MOLLER experiment.

We have also used the AJM model to estimate the magnitude and shape of the inelastic  $ep$  scattering background. Although the AJM model sufficiently constrains the magnitude of this background, a more conservative estimate emphasises the importance of directly monitoring this background within the MOLLER experiment. Conversely, this measurement may serve to better test or constrain the inputs of the AJM model.

## Acknowledgements

We thank K. Kumar for helpful discussions and M. Kuroda for providing code of the colour dipole model parametrisation. N.H. and P.B. thank the Jefferson Lab Theory Center, and W.M. thanks the CSSM/CoEPP at the University of Adelaide and the University of Manitoba for support during visits where some of this work was performed. This work was supported by NSERC (Canada), the DOE Contract No. DE-AC05-06OR23177, under which Jefferson Science Associates, LLC operates Jefferson Lab, and the Australian Research Council through an Australian Laureate Fellowship (A.W.T.), a Future Fellowship (R.D.Y.) and through the ARC Centre of Excellence for Particle Physics at the Terascale.

## References

- [1] C. Y. Prescott, et al., Phys. Lett. B 84 (1979) 524.
- [2] P. A. Souder, et al., Phys. Rev. Lett. 65 (1990) 694.
- [3] K. A. Aniol, et al., Phys. Lett. B 509 (2001) 211.
- [4] K. A. Aniol, et al., Phys. Lett. B 635 (2006) 275.
- [5] D. S. Armstrong, et al., Phys. Rev. Lett. 95 (2005) 092001.
- [6] K. Paschke, A. W. Thomas, R. Michaels, D. Armstrong, J. Phys. Conf. Ser. 299 (2011) 012003.
- [7] R. D. Young, J. Roche, R. D. Carlini, A. W. Thomas, Phys. Rev. Lett. 97 (2006) 102002.
- [8] R. D. Young, R. D. Carlini, A. W. Thomas, J. Roche, Phys. Rev. Lett. 99 (2007) 122003.
- [9] J. Roche, W. T. H. van Oers, R. D. Young, J. Phys. Conf. Ser. 299 (2011) 012012.
- [10] D. Androic, et al., Phys. Rev. Lett. 111 (2013) 141803.
- [11] D. Wang, et al., Phys. Rev. Lett. 111 (2013) 082501.
- [12] J. Mammei, Nuovo Cim. C035N04 (2012) 203.



- [13] P. A. Souder, AIP Conf. Proc. 1441 (2012) 123.
- [14] J. Erler, A. Kurylov, M. J. Ramsey-Musolf, Phys. Rev. D 68 (2003) 016006.
- [15] J. Erler, S. Su, Prog. Part. Nucl. Phys. 71 (2013) 119.
- [16] E. Derman, W. J. Marciano, Annals Phys. 121 (1979) 147.
- [17] A. Czarnecki, W. J. Marciano, Phys. Rev. D 53 (1996) 1066.
- [18] A. Denner, S. Pozzorini, Eur. Phys. J. C 7 (1999) 185.
- [19] F. J. Petriello, Phys. Rev. D 67 (2003) 033006.
- [20] M. Gorchtein, C. J. Horowitz, Phys. Rev. Lett. 102 (2009) 091806.
- [21] A. Sibirtsev, P. G. Blunden, W. Melnitchouk, A. W. Thomas, Phys. Rev. D 82 (2010) 013011.
- [22] B. C. Rislow, C. E. Carlson, Phys. Rev. D 83 (2011) 113007.
- [23] M. Gorchtein, C. J. Horowitz, M. J. Ramsey-Musolf, Phys. Rev. C 84 (2011) 015502.
- [24] P. G. Blunden, W. Melnitchouk, A. W. Thomas, Phys. Rev. Lett. 107 (2011) 081801.
- [25] N. L. Hall, P. G. Blunden, W. Melnitchouk, A. W. Thomas, R. D. Young, Phys. Rev. D 88 (2013) 013011.
- [26] J. Arrington, P. G. Blunden, W. Melnitchouk, Prog. Part. Nucl. Phys. 66 (2011) 782.
- [27] M. E. Christy, P. E. Bosted, Phys. Rev. C 81 (2010) 055213.
- [28] J. Alwall, G. Ingelman, Phys. Lett. B 596 (2004) 77.
- [29] J. J. Sakurai, D. Schildknecht, Phys. Lett. B 40 (1972) 121.
- [30] P. Jimenez-Delgado, W. Melnitchouk, J. F. Owens, J. Phys. G 40 (2013) 093102.
- [31] S. Alekhin, J. Blumlein, S. Moch, Phys. Rev. D 86 (2012) 054009.
- [32] J. Beringer, et al., Phys. Rev. D 86 (2012) 010001.
- [33] D. Androic, et al., arXiv:1212.1637 (2012).
- [34] A. Capella, A. Kaidalov, C. Merino, J. Tran Thanh Van, Phys. Lett. B 337 (1994) 358.
- [35] G. Cvetic, D. Schildknecht, A. Shoshi, Eur. Phys. J. C 13 (2000) 301.
- [36] G. Cvetic, D. Schildknecht, B. Surrow, M. Tentyukov, Eur. Phys. J. C 20 (2001) 77.
- [37] M. Kuroda, D. Schildknecht, Phys. Rev. D 85 (2012) 094001.
- [38] P. G. Blunden, W. Melnitchouk, A. W. Thomas, Phys. Rev. Lett. 109 (2012) 262301.
- [39] P. L. Anthony, et al., Phys. Rev. Lett. 95 (2005) 081601.